

Can Higher-Order Finite-Difference Operators Be Applied across a Material Interface?

Jaroslav Valovcan¹ , Peter Moczo^{*1} , Jozef Kristek¹ , Martin Galis¹ , and Miriam Kristekova² 

ABSTRACT

It is well known that higher-order and thus longer-stencil finite-difference operators (FDOs) can be advantageously used for evaluating spatial derivatives in the finite-difference schemes applied to smoothly heterogeneous media. This is because they reduce spatial grid dispersion. However, realistic models often include sharp material interfaces. Can high-order long-stencil FDOs be applied across such material interface? We address this question by comparing exact spatial derivatives against derivatives approximated by FDOs with respect to the interface representation, velocity contrast, and order of the FDO. The interface is considered in an arbitrary position with respect to the spatial grid. The material interface exactly represented by the Heaviside step function causes a large error of the FDO spatial derivative near the interface. The maximum error near the interface practically does not depend on the order of the FDO. There are only small differences in errors among FDOs of different orders elsewhere. The larger the velocity contrast, the larger the error. If the material interface is represented using a wavenumber band-limited Heaviside function, the error is smoothed and several times smaller. The error in the wavenumber band-limited model decreases with an increasing order of the FDO. Our findings combined with those by Moczo *et al.* (2022) lead to the important conclusion: The wavenumber band-limited representation of the material interface is not only a necessary consequence of discretization of the original physical model but also significantly reduces the error in evaluating a spatial derivative using the FDO.

KEY POINTS

- We address the problem of accuracy of the spatial finite-difference operators across a material interface.
- Accuracy is analyzed with respect to the order of operator, velocity contrast, and interface representation.
- The wavenumber band limitation significantly reduces the error of the spatial derivative by the operator.

INTRODUCTION





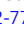
Reduction of grid dispersion

In the finite-difference (FD) method, temporal and spatial derivatives of field variables are replaced by FD operators (FDOs). In most cases, the temporal derivatives are replaced by the centered 2nd-order FDO. The FD schemes mostly differ from one another in FDOs used for spatial derivatives.

The simplest but, at the same time, the least efficient way to approximate a spatial derivative by the FDO is to use the Taylor series. The Taylor series makes it formally possible to obtain FDO of a chosen order, but there are two principal limitations of the implied FD schemes. They are 2nd-order accurate in time, causing a non-negligible temporal dispersion.

A higher order in space reduces spatial dispersion, but this reduction is relatively far from the best possible.

Many approaches have been developed to reduce grid dispersion. Certainly, we should mention the pioneering work by Holberg (1987), who developed optimized spatial FDOs by minimizing peak relative error in group velocity. For recent concise reviews, we refer to Etemadsaeed *et al.* (2016) and Zhou, Liu, and Wang (2022). The latter article provides an overview of a remarkable effort focused on finding optimal FD approximations of the spatial derivatives. The goal of the development is to find FD approximations with (1) the same optional high-order accuracy in space and time in all propagation directions and in a wide range of wavenumbers and (2) optimal balance between increasing order of accuracy and computational demands.

1. Faculty of Mathematics, Physics and Informatics, Comenius University in Bratislava, Bratislava, Slovakia,  <https://orcid.org/0000-0002-7728-2064> (JV);  <https://orcid.org/0000-0001-5276-9311> (PM);  <https://orcid.org/0000-0002-2332-541X> (JK);  <https://orcid.org/0000-0002-5375-7061> (MG); 2. Earth Science Institute, Slovak Academy of Sciences, Bratislava, Slovakia,  <https://orcid.org/0000-0001-9017-5952> (MK)

*Corresponding author: moczo@fmph.uniba.sk

Cite this article as Valovcan, J., P. Moczo, J. Kristek, M. Galis, and M. Kristekova (2023). Can Higher-Order Finite-Difference Operators Be Applied across a Material Interface? *Bull. Seismol. Soc. Am.* **113**, 1924–1937, doi: [10.1785/0120230037](https://doi.org/10.1785/0120230037)

© Seismological Society of America

Important findings on the possibilities to reduce grid dispersion have been recently presented by [Zhou et al. \(2022\)](#). They have emphasized the influence of the spatial grid spacing and time step and demonstrated that without appropriate setting of these parameters, even though the pseudospectral method (equivalent to the infinite-order FD method in space) or k -space method (equivalent to the infinite-order FD method in time and space) is adopted, the simulated acoustic and elastic wavefields in homogeneous media still deviate from the analytical solutions.

With respect to the principal aspect of the approach by [Zhou, Liu, and Wang \(2022\)](#) and important findings by [Zhou et al. \(2022\)](#), let us mention a comprehensive alternative approach developed by [Masson \(2023\)](#)—a distributional FD method. [Masson \(2023\)](#) derived differential operators using a variational approach, independently of the governing equation. One advantage of the approach is that it can be used as an FD method using a few large elements, or as a finite- or spectral-element method in which complex structures in the velocity model are meshed using small elements. Being based on the variational approach, the computational scheme does not include a problem of application of a spatial FDO across the interface.

We should especially mention the approach by [Mora \(1986\)](#) and [Igel et al. \(1995\)](#). They realized that the spatial grid spacing imposes a limit in the wavenumber domain, and the wavenumber band-limited spatial derivative takes a form of a continuous spatial convolution. This convolution should be approximated by a discrete convolution.

In general, and simply said: (a) With a properly chosen spatial grid spacing, the optimized FDOs considerably reduce grid dispersion in homogeneous or smoothly and weakly heterogeneous media; some of the most recent FDOs also reduce temporal dispersion, and (b) a more accurate FDO means a higher order and a larger stencil size.

Material interfaces

Realistic models of the Earth's interior, at all scales, often include material interfaces. [Mittet \(2017\)](#) pointed out cases in seismic exploration in which an accurate description of interface is important (the seabed being a good example). [Moczo et al. \(2018\)](#), based on extensive numerical investigation of an earthquake ground motion in a set of typical sedimentary valleys, demonstrated that the key structural parameters are the shape ratio and overall geometry of the sediment–bedrock interface, impedance contrast at the sediment–bedrock interface, and attenuation in sediments.

Obviously, the legitimate question is: Are the higher-order large-stencil FDOs applicable with the same dispersion-reduction effect also in media with material interfaces, especially sharp high-contrast material interfaces? Can the FDO be applied across the material interface? As far as we know, the relation between the high-order large-stencil FDO and the material interface has not been comprehensively analyzed.

Partial aspects of the problem were probably first mentioned by [Cunha \(1993\)](#). [Mittet \(2017\)](#) explicitly formulated the important question: “What order do we need for the derivative operators to keep dispersion errors less than the errors induced by the interface implementation?” [Jiang and Zhang \(2021\)](#) and [Koene et al. \(2022\)](#) also addressed partial aspects of the problem.

[Cunha \(1993\)](#) pointed out that a long, higher-order FD spatial operator is appropriate for computing a derivative of a continuous function, whereas a short, 2nd-order operator is more suitable for piecewise continuous function. His interest was specific in a sense that he addressed the 2nd-order displacement formulation of the equation of motion that includes spatial derivatives of elastic coefficients.

[Mittet \(2017\)](#) performed an extensive series of numerical tests to answer the question that he formulated. He used a 1D model of two half-spaces and FDOs of different orders for the band-limited Heaviside representation of the interface. Based on the tests, he concluded that a 12th-order Taylor operator is required to keep dispersion errors smaller than the errors due to the interface implementation.

Recently, [Jiang and Zhang \(2021\)](#) applied 14th-order optimal staggered-grid FDOs ([Liu, 2014](#)) in their numerical testing of the accuracy of discrete representations of material interfaces. The reason for using the 14th-order FDO was to suppress the dispersion error so that the “interface error” can dominate the overall error even when coarse grids are used.

Similarly, [Koene et al. \(2022\)](#) used high-order FD spatial operators up to 40th order with large stencil sizes to ensure that no spatial dispersion errors are introduced by the modeling scheme in their numerical testing of the accuracy of discrete representations of material interfaces. In other words, they wanted to isolate errors due to an implementation of the material interface. They compared results obtained using different orders of FDOs and concluded that their findings are not necessarily biased by the large stencil size and the order of the FDO. We refer the reader to the article by [Koene et al. \(2022\)](#), to see the specific way of evaluating accuracy of various implementations of the material interface.

At this stage, we can and, in fact, we have to preliminarily point out that a result of an application of the FDO across the material interface obviously depends on both the FDO itself and the way that the material interface is represented in the FD grid and scheme.

Representations of the material interface in heterogeneous FD schemes

In the heterogeneous FD schemes, FD spatial operators are applied in all interior grid points to calculate spatial derivatives of the wavefield variables. This means that one and the same scheme is used for any interior grid point, no matter what the position of the grid point with respect to the material interface is.

One scheme for any grid point should be a discrete approximation of one formulation (say, a heterogeneous formulation) of the equations of motion and constitutive law for any spatial position in the considered medium. This also means the same form of the equations for a position away from the material interface and a position directly at the material interface. Clearly, the heterogeneous formulation of equations must account for the boundary conditions at the material interface.

Consider a 1D problem in a model of two homogeneous half-spaces with a welded material interface at $z = z_{\text{MI}}$. Material parameters are discontinuous at the material interface. The boundary conditions at the material interface are continuity of the particle velocity v and continuity of stress σ . Spatial derivatives $\partial v/\partial z$ and $\partial \sigma/\partial z$ are discontinuous at the material interface. The velocity–stress heterogeneous formulation may be written as (e.g., [Moczo et al., 2022](#)):

$$\langle \rho \rangle^z \frac{\partial v}{\partial t} = \left\langle \frac{\partial \sigma}{\partial z} \right\rangle^z, \quad \langle C \rangle^z \frac{\partial \sigma}{\partial t} = \left\langle \frac{\partial v}{\partial z} \right\rangle^z. \quad (1)$$

Here, ρ is density, C is compliance, t is time, and $\langle \rangle^z$ indicates the arithmetic averaging. Equation (1) properly ([Backus, 1962](#)) average discontinuous quantities at the material interface, whereas they take the correct forms in each of the two half-spaces.

In most (or all?) FD schemes, the averaging of discontinuous spatial derivatives of the field variables is not explicitly addressed. The so far developed FD schemes differ from each other by evaluating average material parameters.

Evaluation of the average material parameters is relatively easy in the considered 1D problem in which the material interface is parallel with a grid plane. In the staggered grid, an arithmetic average of density is evaluated at a grid point of the particle velocity, and a harmonic average of the elastic modulus (equivalent of the arithmetic average of the compliance) is evaluated at a grid point of stress ([Moczo et al., 2002](#)). In this case, the averaging corresponds to the averaging by [Schoenberg and Muir \(1989\)](#) and [Muir et al. \(1992\)](#), and to the orthorhombic averaging by [Moczo et al. \(2014\)](#) and [Kristek et al. \(2017\)](#)—both approaches applicable in the case of a general position of the interface in the grid.

In the considered 1D case, [Mittet's \(2017, 2021a,b\)](#) representation of the interface using a wavenumber band-limited Heaviside step function is also applicable.

Several FD schemes still use a local pointwise representation (sampling at coarse resolution in the reasonable terminology by [Koene et al., 2022](#)). This representation in principle cannot explicitly account for the boundary conditions.

Spatial discretization and implied wavenumber band limitation

Recently, [Moczo et al. \(2022\)](#) have analyzed consequences of the heterogeneity of the medium, spatial discretization, and the

Nyquist-wavenumber band limitation for the FD modeling of seismic wave propagation and earthquake ground motion. They have found that (1) the grid representation of the material interface must be limited by the Nyquist wavenumber; (2) the wavenumber band limitation replaces spatial derivatives both in the homogeneous medium and across a material interface by continuous spatial convolutions; and (3) the continuous convolution of an infinite spatial extent must be replaced by a finite-extent discrete convolution, that is, by a proper spatial FDO.

Let us mention that [Mittet \(2017\)](#), based on his investigation of the implementation of the sharp material interface using band-limited Heaviside function, concluded that the grid representation of the material interface must be limited by the Nyquist wavenumber. Mittet in his article ([Mittet, 2017](#)) and the follow-up studies ([Mittet, 2021a,b](#)) anticipated several aspects of the analysis by [Moczo et al. \(2022\)](#).

Goal of this article

In the follow-up of the analysis by [Moczo et al. \(2022\)](#), in this article we aim to answer the following questions:

1. May the FDO, which is commonly used for evaluating spatial derivative in a smoothly heterogeneous medium, be also applied across a material interface?
2. How accurate is the FDO derivative in relation to the interface representation? How does it depend on velocity contrast at the interface and the order of the FDO?
3. What are implications for the representation of the material interface?

We compare errors of spatial derivatives obtained using the spatial FDOs of the 4th, 6th, 8th, 10th, and 12th orders across the material interface for two interface representations. In the first one, a sharp material discontinuity is represented using an exact Heaviside step function. In the second one, the same material discontinuity is represented using a wavenumber band-limited Heaviside step function.

Based on the numerical investigations, we formulate implications for the FD modeling of seismic waves and earthquake ground motion in media with material interfaces.

1D PROBLEM FOR A MODEL OF A STACK OF LAYERS BETWEEN TWO HOMOGENEOUS HALF-SPACES: AN EXACT SOLUTION

In this section, we will use the Thomson–Haskell ([Thomson, 1950](#); [Haskell, 1953](#)) propagator matrix method to obtain the exact solution in the 1D multilayered model of medium.

Consider $n - 1$ homogeneous isotropic elastic layers between two homogeneous isotropic elastic half-spaces as shown in Figure 1. A coordinate axis z is oriented positive downward. A thickness of the j th layer is h_j , and velocity and density in the j th layer are c_j and ρ_j , respectively.

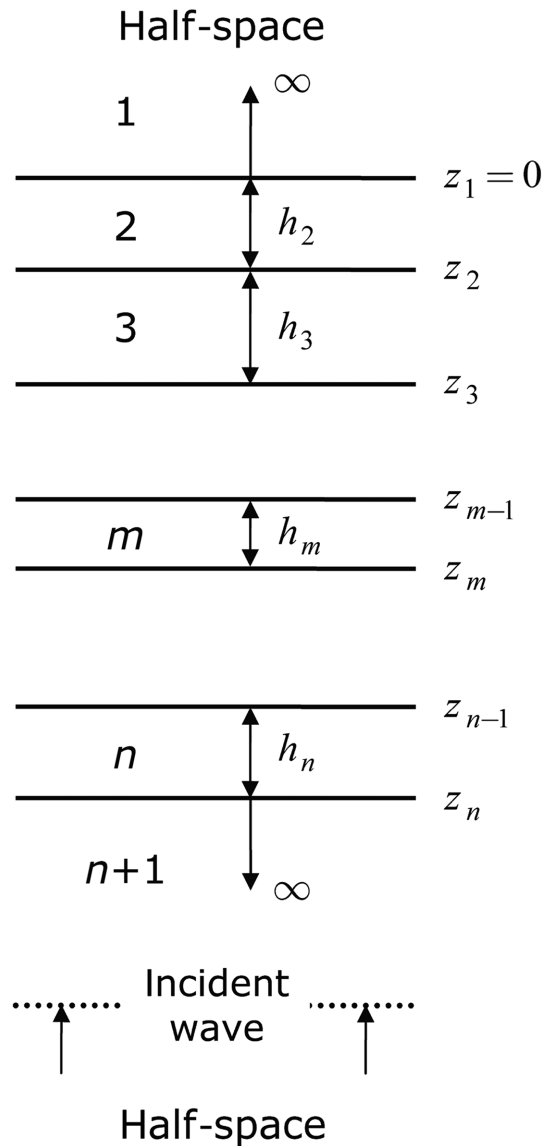


Figure 1. One-dimensional model of a stack of homogeneous isotropic elastic layers between two homogeneous isotropic elastic half-spaces.

Consider 1D harmonic wavefield due to a harmonic plane wave with a unit amplitude propagating in the negative z direction in half-space $n + 1$ with displacement in the form:

$$u^{(n+1)}(z,t) = \exp\left[-i\left(\omega t + \frac{z}{c_{n+1}}\right)\right], \quad (2)$$

with angular frequency $\omega = 2\pi f$. Correspondingly, the Fourier transform and its inverse are defined as

$$\varphi(f) := F\{\varphi(t)\} := \int_{-\infty}^{\infty} \varphi(t) \exp(i2\pi ft) dt, \quad (3)$$

and

$$\varphi(t) := F^{-1}\{\varphi(f)\} := \int_{-\infty}^{\infty} \varphi(f) \exp(-i2\pi ft) df. \quad (4)$$

Assume also a transient wave propagating in half-space $n + 1$ in the negative z direction and entering the stack of layers and half-space 1. Denote a Fourier spectrum of this input wave by $S(f)$.

Displacements in the half-spaces 1 and $n + 1$ are

$$u^{(1)}(z,t) = F^{-1}\{S(f)H^{(1)}(z,f)\}; \quad z \leq 0, \quad (5)$$

$$u^{(n+1)}(z,t) = F^{-1}\{S(f)H^{(n+1)}(z,f)\}; \quad z \geq z_n, \quad (6)$$

in which $H^{(1)}(z,f)$ and $H^{(n+1)}(z,f)$ are the transfer functions:

$$H^{(1)}(z,f) = \frac{2\omega q_{n+1}}{\omega(q_1 A_{22} + q_{n+1} A_{11}) + i(A_{21} - \omega^2 q_1 q_{n+1} A_{12})} \times \exp\left(\frac{-i\omega z}{c_1}\right), \quad (7)$$

$$H^{(n+1)}(z,f) = \left\{ -\frac{BN}{BD} \exp\left[\frac{i\omega}{c_{n+1}}(z - z_n)\right] + \exp\left[-\frac{i\omega}{c_{n+1}}(z - z_n)\right] \right\}, \quad (8)$$

with the wave impedance $q_j = \rho_j c_j$, matrix $\mathbf{A} = \mathbf{A}_n \mathbf{A}_{n-1} \dots \mathbf{A}_2$, layer matrix,

$$\mathbf{A}_j = \begin{bmatrix} \cos b_j & \frac{\sin b_j}{\omega q_j} \\ -\omega q_j \sin b_j & \cos b_j \end{bmatrix}, \quad (9)$$

expressions

$$\begin{aligned} BN &= A_{21} + \omega^2 q_1 q_{n+1} A_{12} + i\omega(q_{n+1} A_{11} - q_1 A_{22}), \\ BD &= A_{21} - \omega^2 q_1 q_{n+1} A_{12} - i\omega(q_{n+1} A_{11} + q_1 A_{22}), \end{aligned} \quad (10)$$

and $b_j = \omega h_j / c_j$.

Spatial derivatives in the two half-spaces are

$$\frac{\partial}{\partial z} u^{(1)}(z,t) = F^{-1}\left\{S(f) \frac{\partial}{\partial z} H^{(1)}(z,f)\right\}; \quad z \leq 0, \quad (11)$$

$$\frac{\partial}{\partial z} u^{(n+1)}(z,t) = F^{-1}\left\{S(f) \frac{\partial}{\partial z} H^{(n+1)}(z,f)\right\}; \quad z \geq z_n, \quad (12)$$

in which

$$\begin{aligned} \frac{\partial}{\partial z} H^{(1)}(z,f) &= \frac{-i\omega}{c_1} \frac{2\omega q_{n+1}}{\omega(q_1 A_{22} + q_{n+1} A_{11}) + i(A_{21} - \omega^2 q_1 q_{n+1} A_{12})} \\ &\times \exp\left(\frac{-i\omega z}{c_1}\right), \end{aligned} \quad (13)$$

$$\frac{\partial}{\partial z} H^{(n+1)}(z, f) = -\frac{i\omega}{c_{n+1}} \left\{ \frac{BN}{BD} \exp\left[\frac{i\omega}{c_{n+1}}(z - z_n)\right] + \exp\left[-\frac{i\omega}{c_{n+1}}(z - z_n)\right] \right\}. \quad (14)$$

Displacement in layer j is

$$u^{(j)}(z, t) = F^{-1}\{S(f)H^{(j)}(z, f)\}; z_{j-1} \leq z \leq z_j; 2 \leq j \leq n. \quad (15)$$

Here,

$$H^{(j)}(z, f) = \left\{ B^+ \exp\left[\frac{i\omega}{c_j}(z - z_{j-1})\right] - B^- \exp\left[-\frac{i\omega}{c_j}(z - z_{j-1})\right] \right\} \times \frac{2\omega q_{n+1}}{B^+ D^- - B^- D^+}, \quad (16)$$

with

$$B^\pm = A_{21}^{(U)} \pm \omega^2 q_1 q_j A_{12}^{(U)} - i\omega(q_1 A_{22}^{(U)} \mp q_j A_{11}^{(U)}), \\ D^\pm = \omega(q_{n+1} A_{11}^{(L)} \pm q_j A_{22}^{(L)}) + i(A_{21}^{(L)} \mp \omega^2 q_j q_{n+1} A_{12}^{(L)}), \quad (17)$$

and

$$\mathbf{A}^{(L)} = \mathbf{A}_n \mathbf{A}_{n-1} \dots \mathbf{A}_j; \quad 2 \leq j \leq n, \\ \mathbf{A}^{(U)} = \mathbf{A}_{j-1} \mathbf{A}_{j-2} \dots \mathbf{A}_2; \quad 3 \leq j \leq n, \\ \mathbf{A}^{(U)} = \mathbf{I}; \quad j = 2, \quad (18)$$

in which \mathbf{I} is an identity matrix.

Spatial derivative in layer j is

$$\frac{\partial}{\partial z} u^{(j)}(z, t) = F^{-1}\{S(f) \frac{\partial}{\partial z} H^{(j)}(z, f)\}; \quad z_{j-1} \leq z \leq z_j; \quad 2 \leq j \leq n, \quad (19)$$

in which

$$\frac{\partial}{\partial z} H^{(j)}(z, f) = \frac{i\omega}{c_j} \left\{ B^+ \exp\left[\frac{i\omega}{c_j}(z - z_{j-1})\right] + B^- \exp\left[-\frac{i\omega}{c_j}(z - z_{j-1})\right] \right\} \times \frac{2\omega q_{n+1}}{B^+ D^- - B^- D^+}. \quad (20)$$

1D PROBLEM FOR A MODEL OF A PLANAR MATERIAL INTERFACE: AN EXACT SOLUTION

The case of two half-spaces can be obtained as a limit case from the previous section for $n + 1 = 2$. We show here the explicit formulas because we will numerically evaluate them.

Displacements in the upper half-space 1 and the lower half-space 2 are

$$u^{(1)}(z, t) = F^{-1}\{S(f)H^{(1)}(z, f)\}; \quad z \leq 0, \quad (21)$$

$$u^{(2)}(z, t) = F^{-1}\{S(f)H^{(2)}(z, f)\}; \quad z \geq 0, \quad (22)$$

in which

$$H^{(1)}(z, f) = \frac{2q_2}{q_1 + q_2} \exp\left(\frac{-i\omega z}{c_1}\right), \quad (23)$$

$$H^{(2)}(z, f) = \frac{q_2 - q_1}{q_2 + q_1} \exp\left(\frac{i\omega z}{c_2}\right) + \exp\left(\frac{-i\omega z}{c_2}\right). \quad (24)$$

The spatial derivatives are

$$\frac{\partial}{\partial z} u^{(1)}(z, t) = F^{-1}\left\{S(f) \frac{\partial}{\partial z} H^{(1)}(z, f)\right\}; \quad z \leq 0, \quad (25)$$

$$\frac{\partial}{\partial z} u^{(2)}(z, t) = F^{-1}\left\{S(f) \frac{\partial}{\partial z} H^{(2)}(z, f)\right\}; \quad z \geq 0, \quad (26)$$

in which

$$\frac{\partial}{\partial z} H^{(1)}(z, f) = \frac{-i\omega}{c_1} \frac{2q_2}{q_1 + q_2} \exp\left(\frac{-i\omega z}{c_1}\right), \quad (27)$$

$$\frac{\partial}{\partial z} H^{(2)}(z, f) = \frac{i\omega}{c_2} \left[\frac{q_2 - q_1}{q_2 + q_1} \exp\left(\frac{i\omega z}{c_2}\right) - \exp\left(\frac{-i\omega z}{c_2}\right) \right]. \quad (28)$$

FDOS APPROXIMATING SPATIAL DERIVATIVES ON A STAGGERED GRID

In a 1D displacement-stress staggered grid, we assume a grid position of stress midway between two grid positions of displacement, and vice versa. Let a grid spacing between two neighboring positions of stress (or two neighboring positions of displacement) be h . For obtaining FDOs of order $M \in \{4, 6, 8, 10, 12\}$, we can use formula presented by Crase *et al.* (1992). Consider function $\psi(z)$ approximated by

$$\psi(z) \approx \sum_{i=1}^M L_i(z) \psi(z_i); \quad L_i(z) := \prod_{j=1, j \neq i}^M \frac{z - z_j}{z_i - z_j}. \quad (29)$$

Its derivative at $z = z_0$ is then

$$\left. \frac{\partial \psi(z)}{\partial z} \right|_{z_0} \approx \sum_{i=1}^M \left. \frac{\partial L_i(z)}{\partial z} \right|_{z_0} \psi(z_i) \\ = \sum_{i=1}^M \left[\sum_{k=1, k \neq i}^M \frac{1}{z_i - z_k} \prod_{j=1, j \neq i, k}^M \frac{z_0 - z_j}{z_i - z_j} \right] \psi(z_i). \quad (30)$$

Denoting

$$a_i := \left. \frac{\partial L_i(z)}{\partial z} \right|_{z_0}, \quad (31)$$

and

$$z_i, z_j, z_k \in \left\{ z_0 \pm \frac{1}{2}h, z_0 \pm \frac{3}{2}h, \dots, z_0 \pm \frac{M-1}{2}h \right\}, \quad (32)$$

we obtain for even M :

$$a_i = \frac{1}{h} \sum_{k \in I_M, k \neq i} \frac{1}{i-k} \prod_{j \in I_M, j \neq i, k} \frac{j}{i-j}, \quad i \in I_M, \quad (33)$$

for

$$I_M := \left\{ \pm \frac{1}{2}, \pm \frac{3}{2}, \dots, \pm \frac{M-1}{2} \right\}. \quad (34)$$

Eventually, define an FDO operator of M th order applied to displacement $u(z, t)$ for obtaining its spatial derivative as

$$\hat{D}_z^M u(z, t) := \sum_{i \in I_M} a_i u(z_i, t); \quad z_i = z + ih. \quad (35)$$

RELATIVE AND ABSOLUTE ERRORS OF FDOs WITH RESPECT TO THE EXACT DERIVATIVES

Denoting spectrum of the transient input signal as $S(f)$ and the transfer function as $H(z, f)$, we may write

$$u(z, t) = F^{-1}\{S(f)H(z, f)\}. \quad (36)$$

A spatial derivative of the exact displacement is

$$\frac{\partial}{\partial z} u(z, t) = F^{-1}\left\{S(f) \frac{\partial}{\partial z} H(z, f)\right\}. \quad (37)$$

An approximate FDO derivative of the exact displacement is obtained using the FDO defined by relation (35).

Let us point out that in the following, we assume that the FDO is at any time applied to the exact displacement. Consequently, an error of the FDO derivative at any time arises only from a single application of the operator.

Errors of the FDO derivative of displacement

Consider an absolute error of the FDO derivative of displacement, that is, a difference between the FDO derivative of displacement and the exact derivative of displacement:

$$AE^M u(z, t) := \hat{D}_z^M u(z, t) - \frac{\partial}{\partial z} u(z, t). \quad (38)$$

Let us emphasize that both the FDO derivative and the exact derivative relate to the same representation of the material interface. This is in agreement with our goal to investigate how accurate the FDO derivative is in relation to the interface representation.

The error of the FDO derivative of displacement can depend on the propagating signal and its frequency content. Therefore, we will derive a relation between the error of the FDO derivative of displacement and an error of an FDO derivative of the transfer function. Then, we will investigate the error of the FDO derivative of the transfer function.

Relation between the error of the FDO derivatives of displacement and transfer function

Using relations (35)–(38), we have

$$AE^M u(z, t) = \sum_{i \in I_M} a_i F^{-1}\{S(f)H(z_i, f)\} - \frac{\partial}{\partial z} F^{-1}\{S(f)H(z, f)\}. \quad (39)$$

Because the order of differentiation and integration can be interchanged, and the inverse Fourier transform is linear, we can write

$$AE^M u(z, t) = F^{-1}\left\{S(f) \left[\sum_{i \in I_M} a_i H(z_i, f) - \frac{\partial}{\partial z} H(z, f) \right]\right\}. \quad (40)$$

Denote

$$\hat{D}_z^M H(z, f) := \sum_{i \in I_M} a_i H(z_i, f), \quad (41)$$

and

$$AE^M H(z, f) := \hat{D}_z^M H(z, f) - \frac{\partial}{\partial z} H(z, f). \quad (42)$$

Then, rewriting equation (40), we obtain a relation between the error of the FDO derivative of displacement and an error of an FDO derivative of the transfer function:

$$AE^M u(z, t) = F^{-1}\{S(f)AE^M H(z, f)\}. \quad (43)$$

Consider a narrowband signal centered at frequency \tilde{f} with an effective width δf . Its amplitude spectrum consists of two identical peaks at frequencies \tilde{f} and $-\tilde{f}$. Because the signal is real, its spectrum has a Hermitian symmetry $S(-f) = S^*(f)$. The transfer function and its derivative are also Hermitian. Therefore, $H(z, -f) = H^*(z, f)$ and $\frac{\partial}{\partial z} H(z, -f) = \frac{\partial}{\partial z} H^*(z, f)$, respectively.

Let us explicitly write the inverse Fourier transform in relation (43):

$$AE^M u(z, t) = \int_{-\infty}^{\infty} S(f) AE^M H(z, f) \exp(-i2\pi f t) df. \quad (44)$$

Accounting for the two spectral peaks, the integral can be approximated by

$$\begin{aligned} \text{AE}^M u(z, t) \approx & S(\tilde{f}) \text{AE}^M H(z, \tilde{f}) \exp(-i2\pi\tilde{f}t) \delta f \\ & + S(-\tilde{f}) \text{AE}^M H(z, -\tilde{f}) \exp(i2\pi\tilde{f}t) \delta f. \end{aligned} \quad (45)$$

Considering the Hermitian symmetry, we have

$$\begin{aligned} \text{AE}^M u(z, t) \approx & S(\tilde{f}) \text{AE}^M H(z, \tilde{f}) \exp(-i2\pi\tilde{f}t) \delta f \\ & + S^*(\tilde{f}) \text{AE}^M H^*(z, \tilde{f}) \exp(i2\pi\tilde{f}t) \delta f. \end{aligned} \quad (46)$$

Since both $S(f)$ and $\text{AE}^M H(z, f)$ are complex, we can write

$$\begin{aligned} S(\tilde{f}) &= A_S(\tilde{f}) \exp[i\varphi_S(\tilde{f})], \\ \text{AE}^M H(z, \tilde{f}) &= A(z, \tilde{f}) \exp[i\varphi(z, \tilde{f})], \end{aligned} \quad (47)$$

and, considering the Hermitian symmetry,

$$\begin{aligned} S^*(\tilde{f}) &= A_S(\tilde{f}) \exp[-i\varphi_S(\tilde{f})], \\ \text{AE}^M H^*(z, \tilde{f}) &= A(z, \tilde{f}) \exp[-i\varphi(z, \tilde{f})]. \end{aligned} \quad (48)$$

Using relations (47) and (48) in equation (46), we obtain

$$\text{AE}^M u(z, t) \approx 2A_S(\tilde{f})A(z, \tilde{f}) \cos[2\pi\tilde{f}t - \varphi_S(\tilde{f}) - \varphi(z, \tilde{f})] \delta f. \quad (49)$$

Obviously, there is a time t_m at which $\text{AE}^M u(z, t)$ reaches its maximum value:

$$\max_t \{\text{AE}^M u(z, t)\} = 2A_S(\tilde{f})A(z, \tilde{f}) \delta f. \quad (50)$$

Both $|\varphi(z, \tilde{f})|$ and $|\varphi_S(\tilde{f})|$ are at most equal to π . Thus, $t_m \in \langle 0, 1/\tilde{f} \rangle \subseteq \langle 0, T \rangle$, in which T is a duration of the signal.

We see that the maximum absolute error of the displacement derivative is proportional to the amplitude of the absolute error of the transfer function derivative. Therefore, we can investigate the error of the transfer function derivative instead of the error of the displacement derivative.

Finally, a broadband signal can be viewed as a signal composed of many narrowband signals centered at different frequencies. Therefore, the maximum absolute error of the displacement derivative is bounded by

$$\max_t \{\text{AE}^M u(z, t)\} \leq 2\delta f \sum_j A_S(\tilde{f}_j)A(z, \tilde{f}_j), \quad (51)$$

in which \tilde{f}_j is the central frequency of the individual narrowband signal of width δf . The inequality is a consequence of a dependence of time t_{mj} at which the maximum is achieved for different frequencies \tilde{f}_j due to a presumed dependence of phases $\varphi(z, \tilde{f}_j)$ on frequencies.

MODELS FOR NUMERICAL INVESTIGATION

In the subsequent section, we present results of investigation of application of the FDOs on the exact values of displacement of

the 1D wavefield in the model of two homogeneous half-spaces with a planar interface being a contact of two half-spaces. We are interested in comparing the derivative obtained using the FDO with the exact spatial derivative at and near the material interface.

We consider four models of two homogeneous half-spaces, symbolically 100/200, 100/300, 200/100, and 300/100. The value in the nominator indicates a wavespeed in the upper half-space, and the value in the denominator indicates the wavespeed in the lower half-space. All values are given in meters per second.

For each model, we consider two representations of the material interface assumed at $z = z_{\text{MI}}$:

1. An exact Heaviside step function,

$$p(z) = p^- \mathcal{H}(z_{\text{MI}} - z) + p^+ \mathcal{H}(z - z_{\text{MI}}), \quad (52)$$

in which $\mathcal{H}(z)$ denotes a Heaviside unit step function, and p^\pm represents a material parameter.

2. A wavenumber band-limited model,

$$p_{k_N}(z) = \frac{1}{2}(p^- + p^+) + (p^+ - p^-) \frac{1}{\pi} \int_0^{k_N(z - z_{\text{MI}})} \frac{\sin u}{u} du, \quad (53)$$

in which k_N denotes the Nyquist wavenumber.

For a detailed explanation of the corresponding theory, we refer to [Moczo et al. \(2022\)](#).

In the wavenumber band-limited models, relation (53) is applied to compliances and densities. Wavespeeds are calculated from the band-limited compliances and densities. The density of 2000 kg/m³ is constant in the entire model, which means there is no difference between an exact and band-limited representation of the density.

In the exact matrix-method calculations, the band-limited model is represented by a layered model consisting of many very thin layers up to distance $8.5h$ to both sides from the interface. At the larger distances, all quantities are constant, being equal to those in the exact model. The configurations with a smaller wavespeed in the upper half-space are shown in Figure 2. The other four configurations are just their mirror images.

NUMERICAL RESULTS

We evaluated approximate derivatives using FDOs of orders 4, 6, 8, 10, and 12. It is sufficient, however, to show results for orders 4, 8, and 12.

Exact and approximate derivatives

Figure 3a,b shows amplitudes of the spatial derivatives of the transfer function $H(z, f)$ as a function of frequency (horizontal axis) and distance from the interface located at $z = 0$ (vertical axis). Though the Nyquist frequency in the slower half-space is

Compliance and wavespeed in the exact and band-limited models

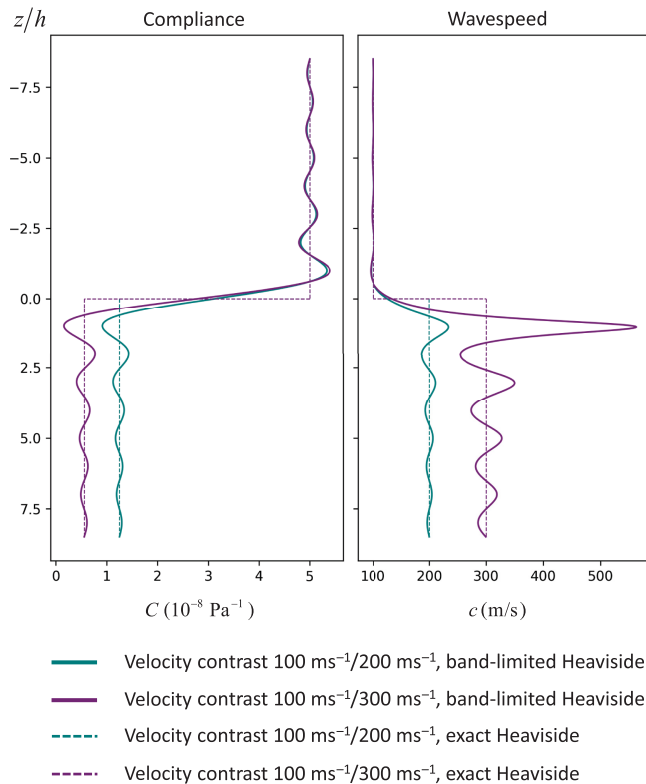


Figure 2. Exact and wavenumber band-limited compliances and corresponding wavespeeds in the models with a lower speed in the upper half-space.

50 Hz, from the practical point of view, it is enough to consider frequencies up to 40 Hz. The distance from the interface is normalized with respect to the grid spacing h . For example, $z/h = 0$ means that the FDO derivative is evaluated at a grid point of stress directly at the interface, that is, using a grid in which the grid point of stress is directly at the interface, and the FDO uses values of displacement at grid points $\pm h/2; \pm 3h/2, \dots$. Distance $z/h = -0.4$, for example, means that the FDO derivative is evaluated at a grid point of stress in the upper half-space at a distance of $0.4h$ away from the interface, that is, using a grid in which the grid point of stress is at the distance of $z/h = -0.4$ from the interface, and the FDO uses values of displacement at grid points $0.1h, -0.9h, 1.1h, -1.9h, \dots$.

We present colormaps only for the 100/200 and 200/100 models because the colormaps for the 100/300 and 300/100 models have analogous structures and differ mainly by a magnitude of amplitudes. Figure 3a relates to the 100/200 model, Figure 3b to the 200/100 model. The upper panels of both figures show derivatives for the exact representation of the interface, and the lower panels show derivatives for the wavenumber band-limited representation.

In the case of the exact representation of the interface, there is a sharp transition between half-spaces in the colormaps of the exact derivatives, whereas the pictures of the FDO

derivatives are blurred. This is a consequence of the fact that an FDO naturally implicitly averages the derivative. The colormaps indicate differences in magnitude of amplitudes of derivatives calculated by FDOs of different orders. This will be better visualized in Figure 4 showing derivatives along the dotted lines, that is, at selected frequencies.

Observe the obvious increase of the amplitude of the spatial derivative with frequency, which is due to the fact that a higher frequency means a shorter wavelength.

We can see the effect of the wavenumber band limitation in Figure 3. The effect can be easily understood. The band limitation removes the discontinuity in material parameters. Consequently, there is no jump in the exact derivative (represented by the sharp transition in the colormaps for the exact representation of the interface), and thus the error of the FDO derivative is reduced near the interface. On the other hand, the band limitation causes variations of the transfer function derivative as a function of distance from the interface. This can be observed well in the upper half-space, in which the transfer function derivative was originally constant from a certain distance away from the interface. This effect is less evident in the lower half-space, because it has an oscillatory character even without band limitation. The oscillatory character of the transfer function in the lower half-space is due to a superposition of the incident and reflected waves.

Let us look at the derivatives at selected frequencies 10, 20, and 30 Hz, indicated by dotted lines in Figure 3a,b. In Figure 4, we can see that there is no large difference among derivatives computed by the FDOs of different orders at lower frequencies. However, we can see that there are differences in the half-space with a lower wavespeed at 30 Hz, and that the accuracy increases with the order of FDO. We will discuss the errors of the FDOs of different orders in detail using the following figures. We can also notice oscillations of the derivative in the upper half-space in the case of the wavenumber band-limited model, and their absence in the case of the exact representation of the interface.

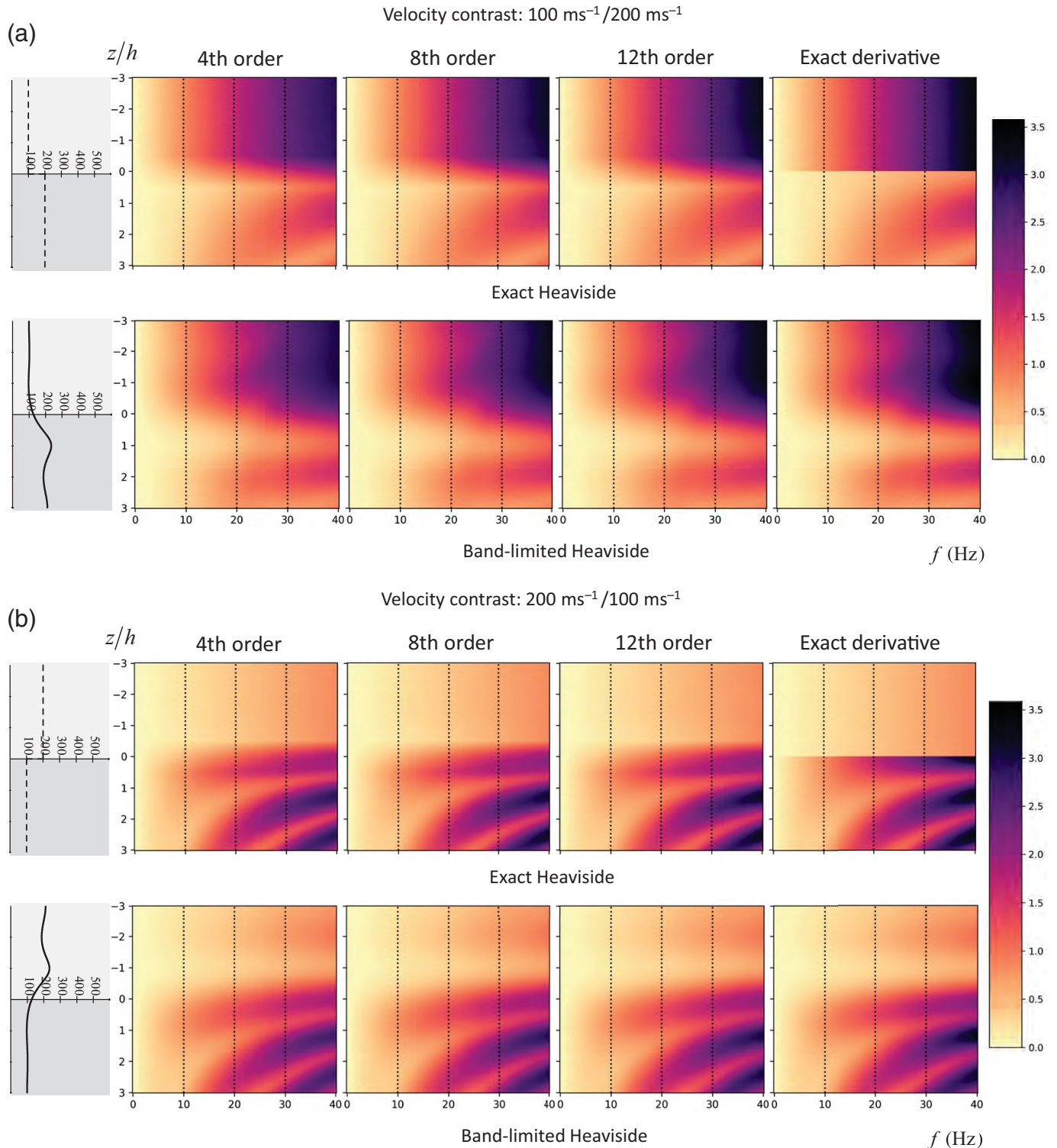
Errors of the FDO derivatives

Figure 5a,b shows amplitudes of the absolute error of the FDO approximations of the transfer function derivatives. The amplitudes are shown as a function of frequency (horizontal axis) and distance from the interface (vertical axis). We can think about the amplitude of the absolute error as of a maximum absolute error over time of a displacement derivative of a narrowband wave with the corresponding central frequency.

Let us observe that the absolute error for a wavenumber band-limited model is defined as a difference of the FDO derivative for the band-limited model and the exact derivative for the same model.

As in Figure 3a,b, we present colormaps only for the 100/200 and 200/100 models because the colormaps for the

Amplitude of the spatial derivative of transfer function

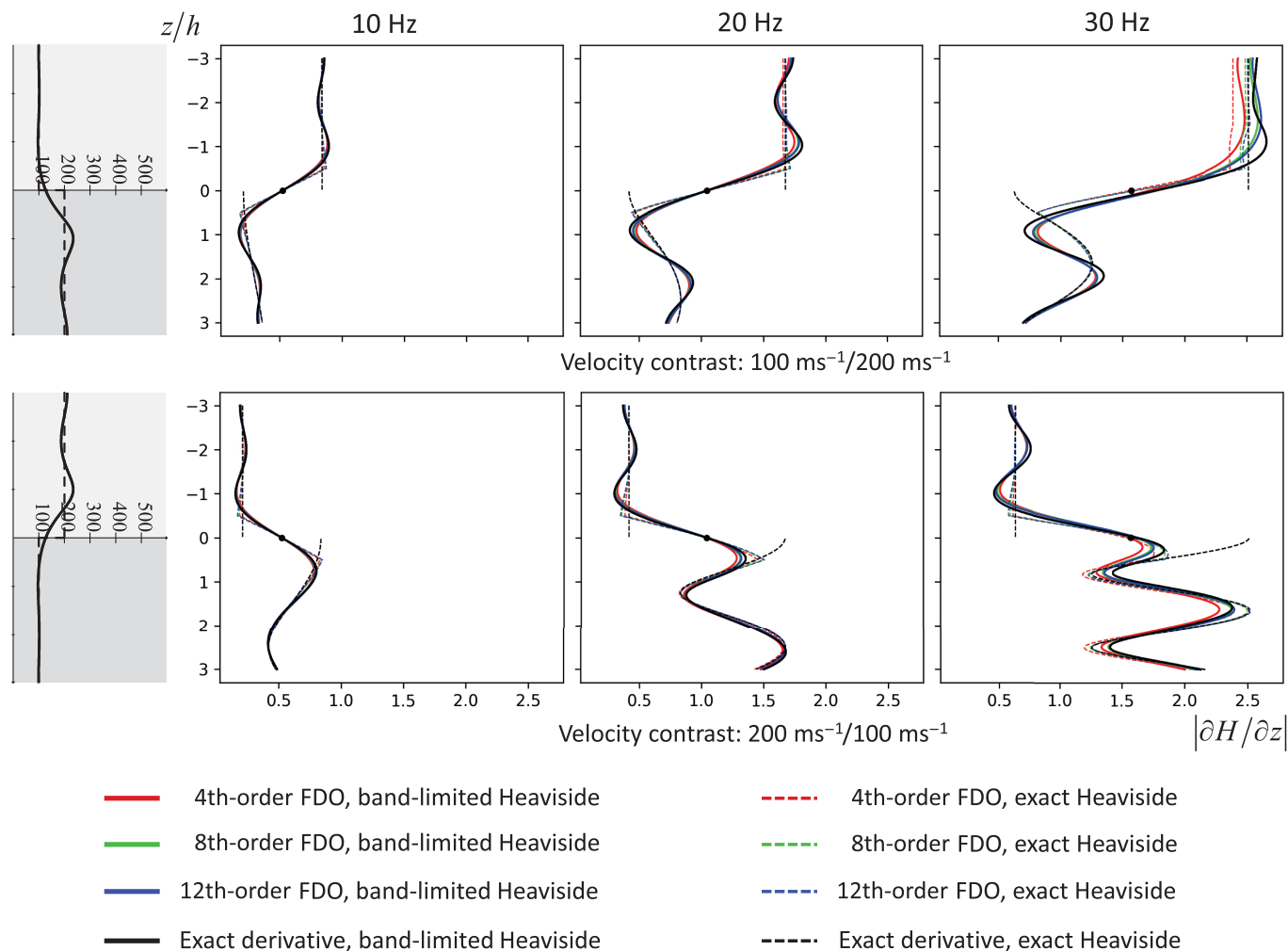


100/300 and 300/100 models have analogous structures and differ mainly by a magnitude of amplitudes.

The first and most important observation is that there is a significant error in the vicinity of the interface in the case of the exact interface representation, which was already indicated in Figure 3a,b. The band limitation significantly (several times)

Figure 3. Amplitude of the spatial derivative of the transfer function of (a) the 100/200 model and (b) the 200/100 model. The upper panel relates to the exact representation of the material interface, and the lower panel relates to the wavenumber band-limited representation. The interface representations and velocity as function of position are indicated at the leftmost subplots. The exact derivative is compared with approximate derivatives obtained using the finite-difference operators (FDOs) of order 4, 8, and 12.

Amplitude of the spatial derivative of transfer function



reduces the absolute error, though the errors are nonzero also at larger distances from the interface. The latter is related to the observed oscillations of the amplitude of the transfer function derivative. Now, we can clearly see that the errors are present on both sides of the interface, not only in the upper half-space. More details can be revealed by looking at the errors at the selected frequencies.

Figure 6a,b shows the amplitude of the absolute error of the transfer function derivative computed by FDOs of different orders at the selected frequencies. Here, we present results for all investigated configurations. Figure 6a shows the amplitude of the absolute error for the 100/200 and 100/300 models, and Figure 6b shows the errors for the 200/100 and 300/100 models. We can immediately see that the larger the velocity contrast, the larger error. The figures well visualize dependence of the errors on the distance from the interface.

First, look at lower frequencies.

Let us start with the exact representation of the interface. The interesting feature is that there is no, or negligible, error directly at the interface. This is because the FDOs properly

Figure 4. Amplitudes of the exact and FDO spatial derivatives of the transfer function at selected frequencies of 10, 20, and 30 Hz. A black circle in the figure indicates the average of the exact derivatives at both sides of the interface.

implicitly average approximate derivatives directly at the interface. Away from the interface to both sides, the error jumps and reaches its largest values. This is because the FDO asymmetrically accounts for displacement values from both sides of the interface.

Subsequently, the error falls linearly to the minima at $z/h = \pm 0.5$. The differences among individual FDO orders are negligible compared to the error magnitude at these distances. Then, the error sharply rises again, though to much lower magnitudes. The larger order of the FDO, the larger error near these local maxima. Furthermore, the error linearly decreases to the minima at $z/h = \pm 1.5$. This pattern of alternating maxima and minima continues at larger distances, however with lower and lower magnitudes, which are practically negligible. The

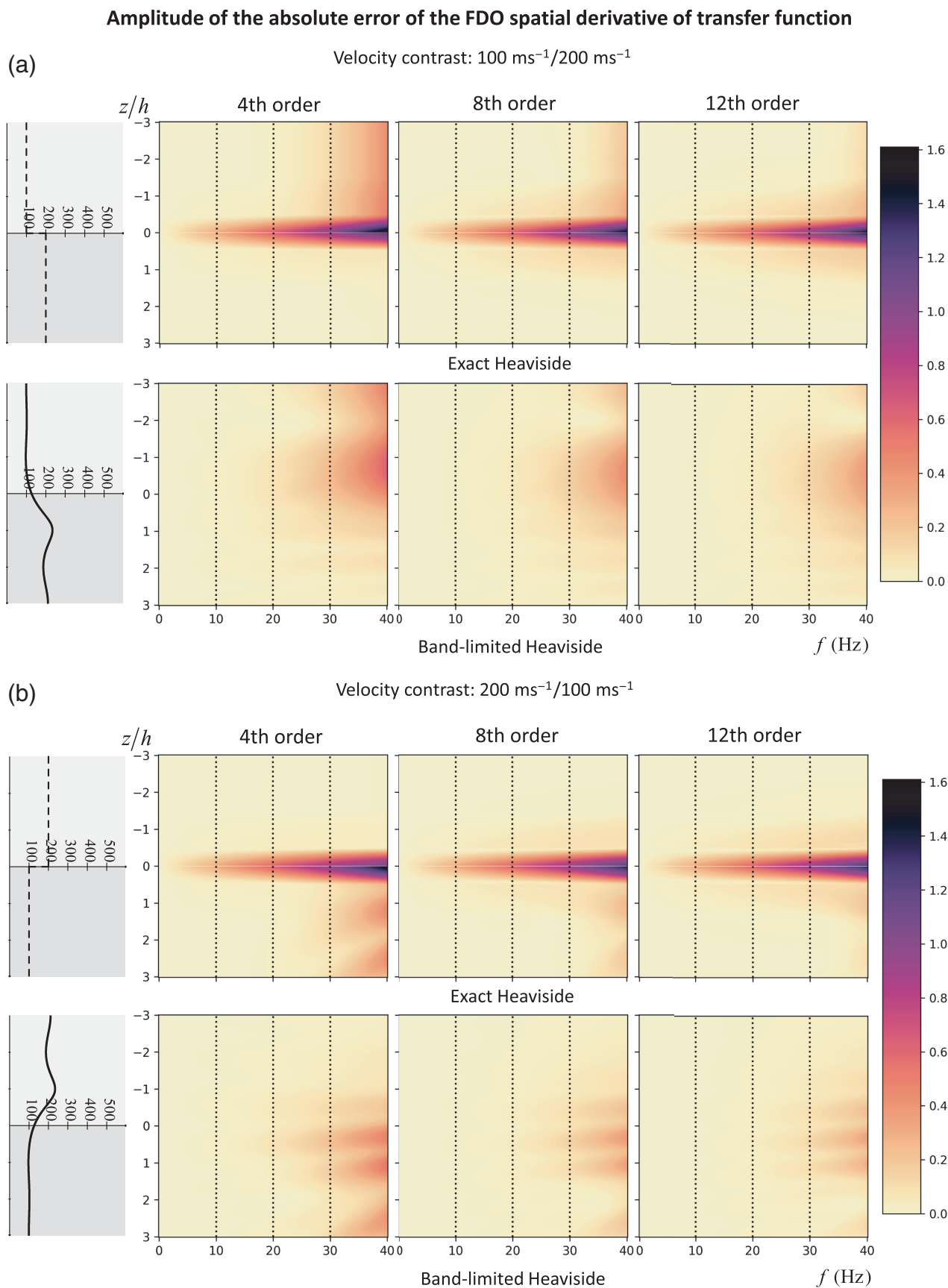


Figure 5. Amplitude of the absolute error of the FDO derivative of the transfer function defined in equation (42). The upper panel relates to the exact

representation, and the lower panel relates to the wavenumber band-limited representation (a) of the 100/200 model and (b) of the 200/100 model.

Amplitude of the absolute error of the FDO spatial derivative of transfer function

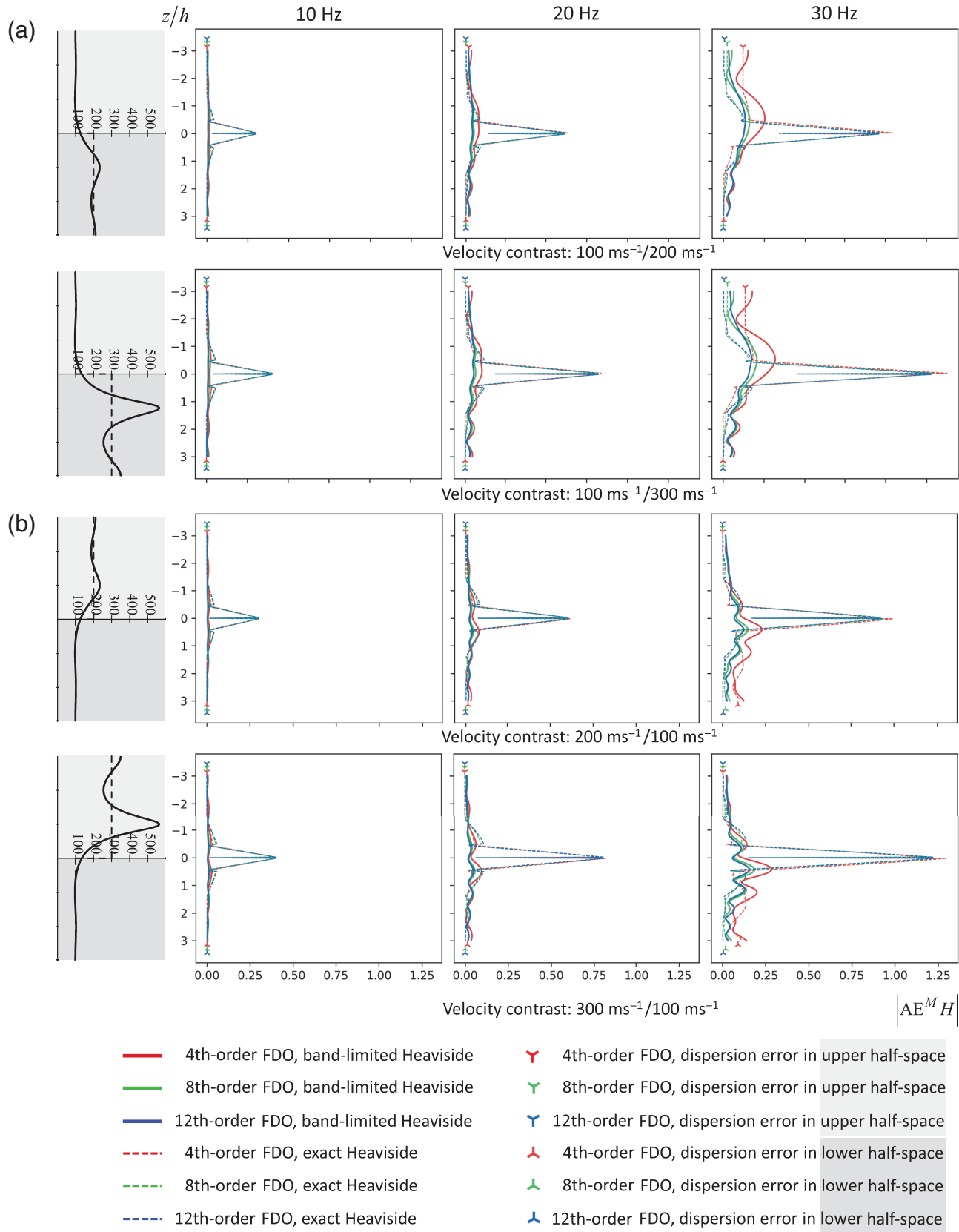


Figure 6. Amplitude of the absolute error of the FDO derivative of the transfer function at selected frequencies (a) for the 100/200 and 100/300 models

and (b) for the 200/100 and 300/100 models.

pattern ends for the 4th-order FDO at the distances $z/h = \pm 1.5$, for the 8th-order FDO at $z/h = \pm 3.5$, and for the 12th-order FDO at $z/h = \pm 5.5$. This can be easily understood because the mentioned distances are the largest distances at which the FDO stencil reaches the interface.

The absolute error in the case of the band-limited representation of the interface is smoothed, compared to the error in the case of the exact interface representation, and is nonzero in the entire model. However, and most important, the error is much smaller at distances in which the error for the exact interface representation is significant, and it is either small or negligible at distances in which the error for the exact representation is negligible or zero. The error decreases with increasing order of the FDO.

Recall that the error is calculated for a single application of the FDO to the exact values of the transfer function. The error is proportional to the maximum error of a single application of the FDO to the exact displacement at the corresponding time. In an FD simulation, the error near the interface would spread over the entire model with time even in the case of the exact interface representation.

Look now at higher frequencies.

As we can see in Figure 5a for the exact interface representation and the 4th-order FDO, there is an error in the upper half-space at distances at which the FDO cannot sense the interface. A similar situation is in Figure 5b for the lower half-space. This error is visible only at higher frequencies. It must be a dispersion-related error.

It can be assumed that the dispersion-related error is present at all other examined FDOs. This means that if we want to investigate only the error due to the interface, we must separate it from the dispersion-related error somehow. For this purpose, we computed the dispersion-related error as the error of the FDO in the homogeneous unbounded model.

In the model with the interface, a transmitted wave propagates in the upper half-space. Therefore, the obtained dispersion-related error must be scaled by the coefficient of transition. The scaled error in the upper half-space is indicated in Figure 6a,b by tri-down symbols placed at the top of the individual subplots. The dispersion-related error decreases with an increasing order of the FDO. We can see that it matches the observed error at larger distances away from the interface. This means that the relatively large error of the FDOs present at high frequencies is the dispersion-related error, not the error due to application of the FDO across the interface. Consequently, we can now understand the error in the case of the exact interface representation. The higher-order FDOs are more accurate at higher frequencies because their dispersion-related error is smaller than that in the lower-order FDOs.

In the lower half-space, the transfer function corresponds to a superposition of the incident and reflected waves. Therefore, both the derivative of the transfer function and the error of the

FDO are not constant. Thus, the error due to the application of the FDO across the interface cannot be separated by subtracting the dispersion-related error. Despite this, we indicate the dispersion-related error by the tri-up symbols placed at the bottom of the individual subplots. We can see that the dispersion-related error gives a good rough estimate of the error of the 4th-order FDO at distances in which the FDO cannot sense the interface. Therefore, we can use the respective dispersion-related error as a reference also for the FDOs of other orders.

Finally, let us comment on the dispersion-related error. It increases with frequency and decreases with an increasing order of the FDOs. It is significant in principle only in the half-space with lower wavespeed. For a fixed frequency of source, and with proper values of the spatial grid spacing and time step, the dispersion-related error is practically negligible for the 12th-order spatial FDO. We assume that this is consistent with the statements by Jiang and Zhang (2021) and Koene *et al.* (2022) in their investigations of discrete representations of the material interface. They used the high-order FDOs to minimize the effect of the grid dispersion in space. Moreover, Koene *et al.* (2022) applied the time-dispersion transform to reduce the error due to the discretization in time.

CONCLUSIONS

A jump in a value of a wavespeed at a material interface exactly represented by the Heaviside step function causes a large error of the spatial derivative evaluated by an FDO near the interface—at distances up to a half grid spacing to both sides from the interface. Recall that the distance here means the distance of a grid point of stress away from the interface at which (the grid point) a spatial derivative is evaluated. The error directly at the interface is negligible.

The maximum error near the interface practically does not depend on the order of the FDO. There are only small differences in errors among FDOs of different orders elsewhere. Whereas a higher-order FDO is more accurate in approximating spatial derivative in a smoothly heterogeneous medium, a higher-order FDO derivative is not in general more accurate compared to a lower-order FDO derivative across the exactly represented material interface. At higher frequencies, in a half-space with a lower wavespeed, a higher-order FDO derivative is more accurate than a lower-order FDO derivative due to a lower dispersion-related error. It is not due to application of the FDO across the interface.

The error increases with increasing velocity contrast at the interface.

The wavenumber band limitation significantly (several times) reduces the error near the interface. It also smooths the spatial dependence of the error. On the other hand, whereas the spatial extent of the error in the case of the exact interface representation is limited only up to a certain distance from the interface, the error in the case of the band-limited

representation spatially extends to the entire model. Fortunately, the error introduced due to the wavenumber band limitation is either small or negligible.

The error in the wavenumber band-limited model decreases with an increasing order of the FDO.

The main conclusion for the FD modeling of seismic waves is: The wavenumber band limitation of the heterogeneous model is not only a necessary consequence of discretization of the original physical model, as anticipated by [Mittet \(2017\)](#) treatment of a material interface and shown by [Moczo et al. \(2022\)](#) analysis of the entire equation of motion, but also significantly reduces the error in evaluating a spatial derivative using the FDO across the material interface. A proper band limitation is a necessary condition for obtaining good simulation results.

DATA AND RESOURCES

No data are used in this study.

DECLARATION OF COMPETING INTERESTS

The authors acknowledge that there are no conflicts of interest recorded.

ACKNOWLEDGMENTS

The authors very much appreciate corrections and suggestions provided by the anonymous reviewer and by Rune Mittet. They helped them to improve this article. The authors also appreciate the constructive help and advice by the BSSA Associate Editor Arben Pitarka. This work was supported by the Slovak Research and Development Agency under the Contract APVV-15-0560 (project ID-EFFECTS) and by the Slovak Foundation Grant VEGA 2/0046/20.

REFERENCES

- Backus, G. E. (1962). Long-wave elastic anisotropy produced by horizontal layering, *J. Geophys. Res.* **67**, 4427–4440.
- Crase, E., C. Wideman, M. Noble, and A. Tarantola (1992). Nonlinear elastic wave-form inversion of land seismic-reflection data, *J. Geophys. Res.* **97**, 4685–4703.
- Cunha, C. A. (1993). Elastic modeling in discontinuous media, *Geophysics* **59**, 1840–1851.
- Etemadsaeed, L., P. Moczo, J. Kristek, A. Ansari, and M. Kristekova (2016). A no-cost improved velocity-stress staggered-grid finite-difference scheme for modelling seismic wave propagation, *Geophys. J. Int.* **207**, 481–511.
- Haskell, N. A. (1953). Dispersion of surface waves on multilayered media, *Bull. Seismol. Soc. Am.* **43**, 17–34.
- Holberg, O. (1987). Computational aspects of the choice of operator and sampling interval for numerical differentiation in large-scale simulation of wave phenomena, *Geophys. Prospect.* **35**, 629–655.
- Igel, H., P. Mora, and B. Rioulet (1995). Anisotropic wave propagation through finite-difference grids, *Geophysics* **60**, 1203–1216.
- Jiang, L., and W. Zhang (2021). TTI equivalent medium parametrization method for the seismic waveform modelling of heterogeneous media with coarse grids, *Geophys. J. Int.* **227**, 2016–2043.
- Koene, E. F. M., J. Wittsten, and J. O. A. Robertsson (2022). Finite-difference modelling of 2-D wave propagation in the vicinity of dipping interfaces: A comparison of anti-aliasing and equivalent medium approaches, *Geophys. J. Int.* **229**, 70–96.
- Kristek, J., P. Moczo, E. Chaljub, and M. Kristekova (2017). An orthorhombic representation of a heterogeneous medium for the finite-difference modelling of seismic wave propagation, *Geophys. J. Int.* **208**, 1250–1264.
- Liu, Y. (2014). Optimal staggered-grid finite-difference schemes based on least-squares for wave equation modelling, *J. Geophys. Int.* **197**, 1033–1047.
- Masson, Y. (2023). Distributional finite-difference modelling of seismic waves, *Geophys. J. Int.* **233**, 264–296.
- Mittet, R. (2017). On the internal interfaces in finite-difference schemes, *Geophysics* **82**, T159–T182.
- Mittet, R. (2021a). On the pseudospectral method and spectral accuracy, *Geophysics* **86**, T127–T142.
- Mittet, R. (2021b). Small-scale medium variations with high-order finite-difference and pseudospectral schemes, *Geophysics* **86**, T387–T399.
- Moczo, P., J. Kristek, P.-Y. Bard, S. Stripajová, F. Hollender, Z. Chovanová, M. Kristeková, and D. Sicilia (2018). Key structural parameters affecting earthquake ground motion in 2D and 3D sedimentary structures, *Bull. Earthq. Eng.* **16**, 2421–2450.
- Moczo, P., J. Kristek, and M. Galis (2014). *The Finite-Difference Modelling of Earthquake Motions: Waves and Ruptures*, Cambridge University Press, Cambridge, United Kingdom.
- Moczo, P., J. Kristek, M. Kristekova, J. Valovcan, M. Galis, and D. Gregor (2022). Material interface in the finite-difference modeling: A fundamental view, *Bull. Seismol. Soc. Am.* **113**, 281–296.
- Moczo, P., J. Kristek, V. Vavryčuk, R. J. Archuleta, and L. Halada (2002). 3D heterogeneous staggered-grid finite-difference modeling of seismic motion with volume harmonic and arithmetic averaging of elastic moduli and densities, *Bull. Seismol. Soc. Am.* **92**, 3042–3066.
- Mora, P. (1986). Elastic finite differences with convolutional operators, *Stanford Explor. Proj. Rep.* **48**, 277–289.
- Muir, F., J. Dellinger, J. Etgen, and D. Nichols (1992). Modeling elastic fields across irregular boundaries, *Geophysics* **57**, 1189–1193.
- Schoenberg, M., and F. Muir (1989). A calculus for finely layered anisotropic media, *Geophysics* **54**, 581–589s.
- Thomson, W. (1950). Transmission of elastic waves through a stratified solid medium, *J. Appl. Phys.* **21**, 89–93.
- Zhou, H., Y. Liu, and J. Wang (2022). Elastic wave modeling with high-order temporal and spatial accuracies by a selectively modified and linearly optimized staggered-grid finite-difference scheme, *IEEE Trans. Geosci. Remote Sens.* **60**, 1–22.
- Zhou, H., Y. Liu, J. Wang, and Y. Ma (2022). Novel first-order k-space formulations for wave propagation by asymmetrical factorization of space-wavenumber domain wave propagators, *Geophysics* **87**, T417–T433.

Manuscript received 9 March 2023

Published online 6 June 2023